Exotic Topological Insulator States and Topological Phase Transitions in $Sb_2Se_3-Bi_2Se_3$ Heterostructures

Qianfan Zhang,[†] Zhiyong Zhang,[‡] Zhiyong Zhu,[§] Udo Schwingenschlögl,[§] and Yi Cui[†,⊥,*]

[†]Department of Material Sciences and Engineering and [‡]Stanford Nanofabrication Facility, Stanford University, Stanford, California 94305, United States, [§]PSE Division, KAUST, Thuwal 23955-6900, Saudi Arabia, and [⊥]Stanford Institute for Materials and Energy Sciences, SLAC National Accelerator Laboratory, 2575 Sand Hill Road, Menlo Park, California 94025, United States

ABSTRACT

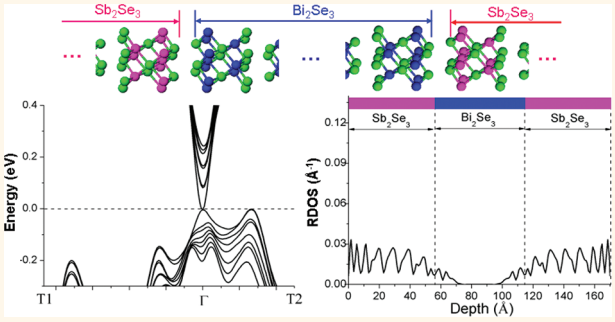

Topological insulator is a new state of matter attracting tremendous interest due to its gapless linear dispersion and spin momentum locking topological states located near the surface. Heterostructures, which have traditionally been powerful in controlling the electronic properties of semiconductor devices, are interesting for topological insulators. Here, we studied the spatial distribution of the topological state in $Sb_2Se_3-Bi_2Se_3$ heterostructures by first-principle simulation and discovered that an exotic topological state exists. Surprisingly, the state migrates from the nontrivial Bi_2Se_3 into the trivial Sb_2Se_3 region and spreads across the entire Sb_2Se_3 slab, extending beyond the concept of "surface" state while preserving all of the topological surface state characteristics. This unusual topological state arises from the coupling between different materials and the modification of electronic structure near Fermi energy. Our study demonstrates that heterostructures can open up opportunities for controlling the real-space distribution of the topological state and inducing quantum phase transitions between topologically trivial and nontrivial states.

KEYWORDS: topological insulator · heterostructure · topological state · first-principle simulation · spin–orbit coupling · quantum phase transition

Following the discovery of two-dimensional (2D) topological insulator (TI) quantum well materials,[1,2] three-dimensional (3D) TI materials represent another significant novel discovery.[3–7] TIs arise from strong atomic spin–orbit coupling (SOC). Strong 3D TI materials are insulating in the bulk region yet metallic on the surface boundary. The gapless boundary states, well-known as topological surface states, have exciting topological properties, such as linear dispersion and spin momentum locking,[8–10] are robust against disorder, and are protected by time-reversal symmetry.[4–6,11,12]

Heterostructures, consisting of materials with distinct band structures, can achieve control of the electronic state and thus carrier transport, modulating the fundamental physical parameters inside the semiconductor devices such as band gap or effective mass.[13,14] Exciting examples include the following: the Si/SiO_2 heterostructure settled the foundation for the modern semiconductor technology; GaAs/AlGaAs quantum wells, due to perfect lattice match, became promising electronic devices with well carrier confinement and high electron mobility;[15–17] the quantum cascade laser, initially realized in the AlInAs/GaInAs coupled quantum well, extends the laser electromagnetic spectrum to the mid- to far-infrared portion of the electromagnetic spectrum.[18] Now heterostructures are widely applied in semiconductor lasers,[19] high-speed bipolar transistors,[20] photonic crystals,[21] and other novel electronic devices.[22,23]

Recently, various heterostructure-like tems composed of topological insulator and trivial materials have attracted great interest because exotic features can be induced through the interface correspondence between topologically nontrivial and topologically trivial phases, due to the existence of a topological surface state. A large number of works, based on the consideration of model Hamiltonians with variable parameters, have predicted such proximity effect induced topological properties, such as one-dimensional fermionic excitations on the dislocation line in TI,[24,25] image magnetic monopole effects on the interface between TI and ferromagnetic materials,[26]

* Address correspondence to yicui@stanford.edu.

Received for review November 21, 2011 and accepted February 17, 2012.

Published online February 17, 2012
10.1021/nn2045328

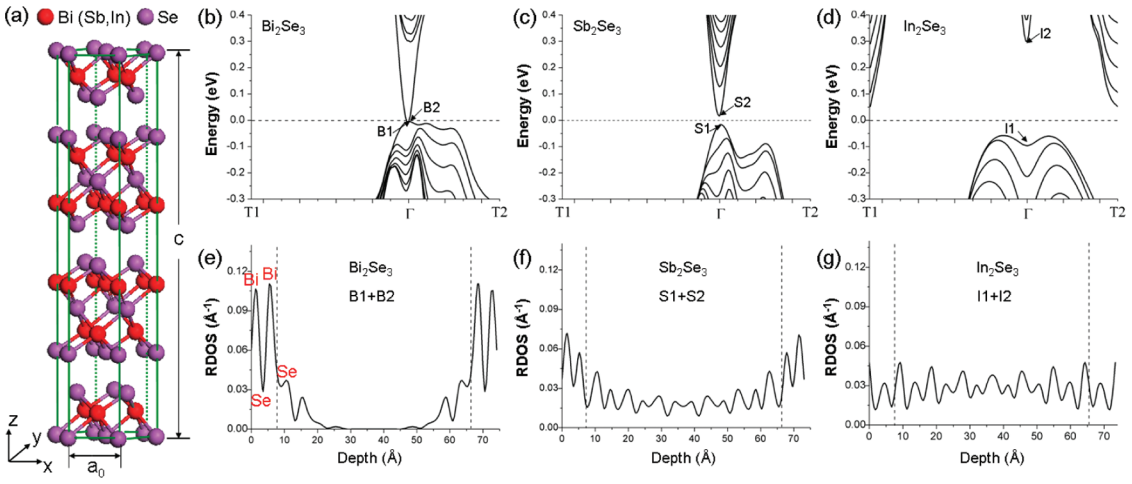

Figure 1. Comparison between Bi_2Se_3, Sb_2Se_3, and In_2Se_3. (a) Layered Bi_2Se_3 or Sb_2Se_3 crystal structure. Bi (or Sb) atoms and Se atoms are marked by red and purple balls, respectively. (a,c) Lattice constants in the hexagonal cell. (b−d) Band structures for 8 QL Bi_2Se_3, Sb_2Se_3, and In_2Se_3 nanoslabs, and the dashed horizontal line shows the position of Fermi energy. (e−g) Closest to Fermi real-space charge density of the states (RDOS). The RDOS is defined as charge density integration of a state on $x-y$ plane at the specified depth z ($z = 0$ is the position of the top Se layer): $P(z) = \int|\psi(x,y,z)|^2 dxdy$. Here, closest to Fermi RDOS is the summations of RDOS for the highest valence state and lowest conduction state at Γ point (B1 + B2 for Bi_2Se_3, S1 + S2 for Sb_2Se_3, and I1 + I2 for In_2Se_3). The dashed vertical lines separate the top or bottom quintuple layer from the inner region.

and Majorana Fermions on the interface between TI and a s-wave superconductor.[27,28] However, due to the complexity of the coupling interaction, it is still hard to unequivocally illustrate the effects of general interfacial interactions in these heterostructures. Furthermore, the real-space distribution of topological surface states is critical to the interfacial interaction, although not enough attention has been paid to this issue. Interfacial interaction can also influence the real-space distribution of topological states. Because the topological states are induced by the transition from a nontrivial to a trivial phase across the boundary, it is commonly believed that the states appear locally as 2D states near the interface on the nontrivial phase side.[26−29] From the computational simulation aspect, although some works have studied the spatial distribution of topological surface states on the TI's surface,[30,31] such analysis has not been performed on heterostructures.

In this work, we investigate topological states in nontrivial−trivial heterostructures by the accurate *ab initio* density functional theory approach. Bi_2Se_3 and Sb_2Se_3, possessing a similar crystal structure and lattice constant in the $x-y$ plane,[5,32] are chosen to construct the heterostructures. They have the rhombohedral structure with space group $D^5_{3d}(R3)$. As shown in Figure 1a, the system has a layered structure with five atomic layers as a basic unit, named a quintuple layer (QL), and the crystal structure is formed by the relatively strong covalent bond within a QL and the weak van der Waals interaction between QLs. Furthermore, the electronic structures of Sb and Bi are similar, and strong interactions near the Fermi level between Bi_2Se_3 and Sb_2Se_3 are expected. Sb and Bi belong to the same group, and Bi lies below Sb. Bi is the heaviest element with stable isotopes, and the relativistic effect causes more contraction of the outer electron shells, which greatly cancels the trend of shell expansion when going down the same group in the periodic table and results in very similar electronegativity and atomic radius with those for Sb. However, Sb_2Se_3 is a trivial insulator, whereas Bi_2Se_3 is a topological insulator due to much stronger SOC effect in Bi atoms.[5,30]

RESULTS AND DISCUSSION

First, we computed the electronic band structures for Bi_2Se_3 and Sb_2Se_3 as a reference to confirm their topological nature. Eight QL (~8 nm thick) nanoslabs, which are thick enough to avoid considerable coupling between the top and bottom surface, were used.[33,34] For the Bi_2Se_3 nanoslab (Figure 1b), a linearly dispersive Dirac cone with a Dirac point at the Γ point exists between the bulk valence band and the bulk conduction band. This gapless state is the topological surface state. However, for the Sb_2Se_3 nanoslab (Figure 1c), an energy gap exists. Thus, Sb_2Se_3 is a trivial insulator. Our simulation results agree well with previous simulation studies[5,30] and experimental results.[10−12]

The topological difference between Bi_2Se_3 and Sb_2Se_3 can also be analyzed by the real-space charge density of the states (RDOS) located closest to the Fermi energy (closest to Fermi RDOS, defined in the caption of Figure 1). Figure 1e,f plots the closest to Fermi RDOS for both slabs, respectively. For Bi_2Se_3, the B1 and B2 states are degenerate at the Dirac point (Figure 1e). These states are real surface states because the charge density is mainly concentrated inside the top and bottom QLs, with minimal penetration into the second outermost QL dropping quickly to zero within the inner region. The TI surface states reside nearly completely in the two outermost QLs and spread only

2 nm in depth from the surface. Interestingly, the density peaks appear at the Bi atoms, presumably due to the strong SOC effect of Bi atoms. In contrast, the closest to Fermi states, S1 and S2, in Sb_2Se_3 (Figure 1f) are not real surface states, and the charge density is nonzero even in the middle of the slab far from the surface. Therefore, the RDOS shape can be viewed as a reasonable characterization method for the real-space properties of the topological surface state. In the following study, this method will be repeatedly applied to study the topologically nontrivial property and visualize the real-space density distribution.

We simulated four types of $Sb_2Se_3-Bi_2Se_3-Sb_2Se_3$ heterostructured slabs with one, two, three, and six Sb_2Se_3 QLs on the top and bottom surfaces of six Bi_2Se_3 QLs. It has been demonstrated, both theoretically and experimentally,[33,34] that a slab with six QLs of Bi_2Se_3 alone has a gapless Dirac cone. As shown in Figure 2a,d, f,i, the gapless surface states exist for all four types of heterostructured slabs, which indicates that the topologically nontrivial states do not disappear when coating Sb_2Se_3 (trivial insulator) onto Bi_2Se_3 (nontrivial insulator). This is expected because the time-reversal symmetry is not violated. However, it is surprising when looking at the real-space distribution of topological states (Figure 2c,e,h,j). The topological states always concentrate inside the trivial Sb_2Se_3 slabs, as shown by the topological RDOS curves. The dominant concentration of topological states in Sb_2Se_3 QLs is true for all four types of heterostructured slabs with different thicknesses of Sb_2Se_3. When coating 1 QL of Sb_2Se_3 on both surfaces (Figure 2c), the shape of charge density is similar to that in uncoated Bi_2Se_3, although the largest peaks locate at the Sb atoms instead of Bi atoms. For 2 QLs (~2 nm), 3 QLs (~3 nm), and 6 QLs (~6 nm) of Sb_2Se_3 coating (Figure 2e,h,j), the surface states spread throughout the entire region of the Sb_2Se_3 slabs and extend very little into the Bi_2Se_3 region. Compared to slabs of Bi_2Se_3 alone, where the 2D topological states are distributed within only 2 QLs (~2 nm) below the surface and are truly "surface states", the heterostructures show two surprising properties of their topological states. First, there exists a quantum topological phase transition, in which trivial Sb_2Se_3 transforms into the nontrivial phase and nontrivial Bi_2Se_3 transforms reversibly into the trivial phase. Second, to the extent of 6 QL Sb_2Se_3 coatings, the topological states in the heterostructures are distributed "bulk-like" instead of localizing only at the surface.

To determine whether the gapless states inside the Sb_2Se_3 layers of heterostructures have topological nature, we also calculated the spin polarization in the Dirac cone, which is the strongest evidence of nontrivial topological character.[19−21,30] Figure 2b,g shows the spin orientation on the gapless states in the 1 QL and 3 QL Sb_2Se_3 coating cases. It can be found that the equal energy surface and spin textures for two states are quite similar. Both energy surfaces are nearly perfect circles; the spin lies in the plane; while moving around the Fermi surface, the spin orientation rotates simultaneously, forming a left-handed spin−orbit ring. Therefore, despite the dramatic quantum topological phase transition in heterostructures, the topological states retain all of the characteristics of the topological Dirac cone.

To elucidate the origin of the surprising topological insulator states in $Sb_2Se_3-Bi_2Se_3-Sb_2Se_3$ heterostructures, we carried out comparative studies on $In_2Se_3-Bi_2Se_3-In_2Se_3$ heterostructures. As shown in Figure 1d,g, In_2Se_3 is a trivial insulator with the same crystal structure as Bi_2Se_3 and Sb_2Se_3. When coating 1 QL, 2 QL, and 3 QL In_2Se_3 on the surfaces of Bi_2Se_3, the gapless topological state always exists (Figure 3a,c,e). For all cases (Figure 3b,d,f), the wave functions of the surface states concentrate in the top QL and bottom QL of the Bi_2Se_3 slab, penetrating only slightly into the In_2Se_3 region. In contrast to $Sb_2Se_3-Bi_2Se_3-Sb_2Se_3$, the topological states of $In_2Se_3-Bi_2Se_3-In_2Se_3$ heterostructures are only ordinary topological interface states with similar nature to the Bi_2Se_3 surface states (the vacuum−Bi_2Se_3 interface states).

To understand the fundamental distinction between these two heterostructures, we analyze the near-Γ atomic orbital partial density state in energy space (PDOS, defined in the caption of Figure 4). We qualitatively studied characteristics of band states near the Fermi energy in three kinds of heterojunctions: (a) 3 QL Sb_2Se_3 coated Bi_2Se_3 (3S−B junction); (b) decoupled 3 QL Sb_2Se_3 coated Bi_2Se_3 (d3S−B junction), where the width of the van der Waals gap between Sb_2Se_3 and Bi_2Se_3 is artificially extended from the equilibrium length $d \sim 2.5$ Å to a larger one $d \sim 3.0$ Å in order to weaken the interaction between two materials; (c) 3 QL In_2Se_3 coated Bi_2Se_3 (3I−B junction). In the decoupled d3S−B junction, as shown in the RDOS curve in Figure 4f, the topological state remains in the Bi_2Se_3 region, similar to the vacuum−Bi_2Se_3 systems, which indicates that a topological phase transition takes place when the interaction between Sb_2Se_3 and Bi_2Se_3 increases. Therefore, 3S−B and d3S−B junctions can serve as good models to study the mechanism of topological phase transitions. Without the SOC effect in either 3S−B (Figure 4a) or d3S−B (Figure 4d) junctions, the Se orbital with negative parity occupies the top of valence band region, and Bi and Sb orbitals with positive parity occupy the bottom of conduction band region. In the d3S−B heterojunction (Figure 4d), when Sb_2Se_3 and Bi_2Se_3 decouple, the Se orbital in Bi_2Se_3 (labeled as Se1) sits on the top of the valence band while the Se orbital in Sb_2Se_3 (labeled Se2) locates below it, and the near-Fermi level orbital forms a Se2−Se1−Sb−Bi order. However, in the 3S−B junction (Figure 4a), when Sb_2Se_3 and Bi_2Se_3 couple, the Se1

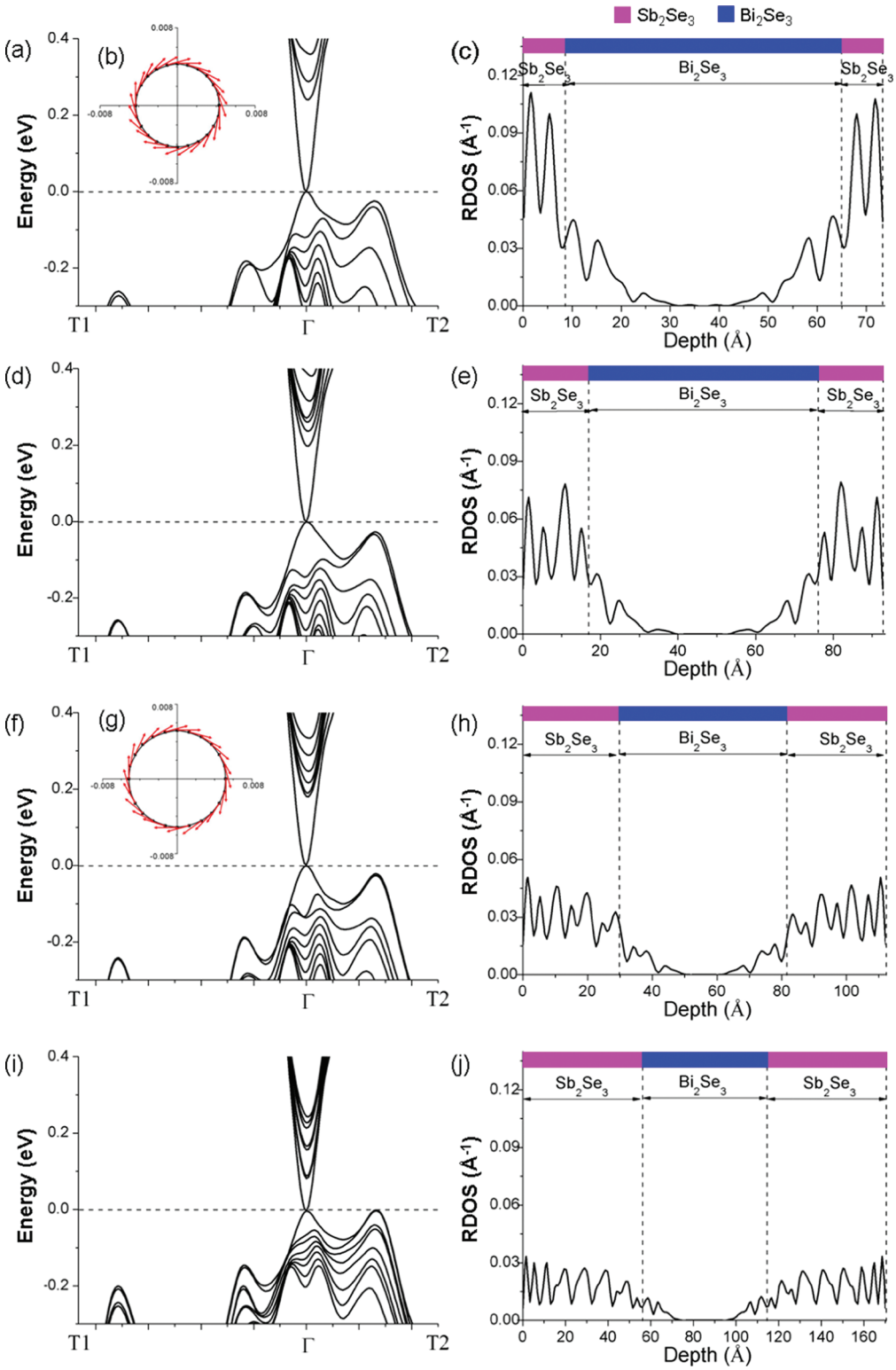

Figure 2. Topological surface state in $Sb_2Se_3-Bi_2Se_3-Sb_2Se_3$ sandwich slabs with different Sb_2Se_3 thickness. (a,d,f,i) Band structures with one, two, three, and six Sb_2Se_3 QLs on each surface of six QL Bi_2Se_3 slabs, respectively. (c,e,h,j) Closest to Fermi RDOS for these sandwich slabs. The dashed vertical lines are the boundaries between Sb_2Se_3 and Bi_2Se_3, and the purple and blue bars represent the Sb_2Se_3 and Bi_2Se_3 slab regions. (b,g) Equal energy surfaces at $E = 0.045$ eV for 1 QL and 3 QL Sb_2Se_3 coating cases (momentum unit: $2\pi/a$ Å^{-1}, a is the lattice constant). Energy surfaces are presented by black circles. In-plane spin orientations are denoted by red arrows.

and Se2 orbitals strongly interact and the Se2 orbital dominates the edge of the valence band, so the state order changes to Se1−Se2−Sb−Bi. By turning on the SOC effect, band inversion occurs between the Bi and

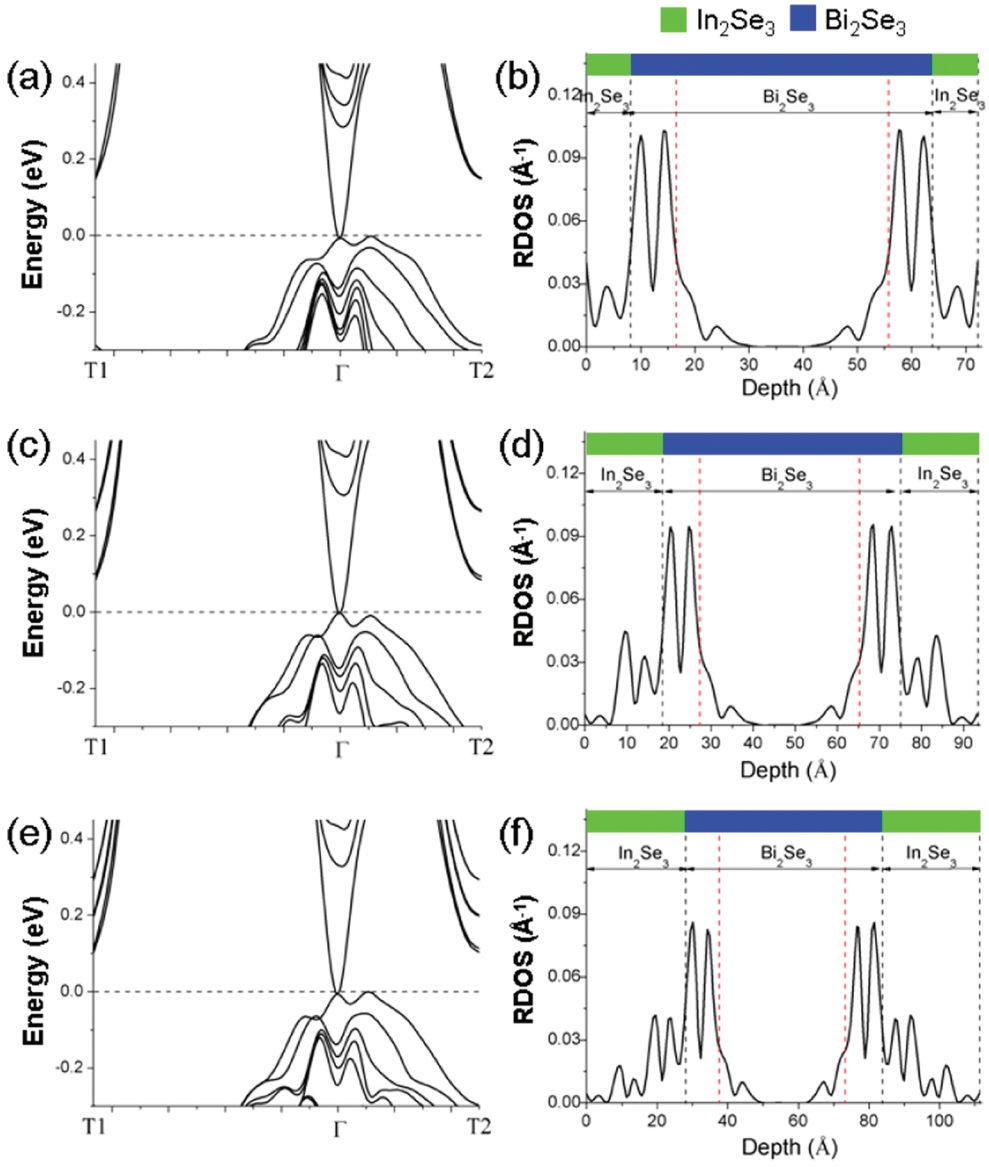

Figure 3. Topological surface state in In_2Se_3−Bi_2Se_3−In_2Se_3 sandwich slabs with different In_2Se_3 thickness. (a,c,e) Band structures with one, two, and three In_2Se_3 quintuple layers on each surface of Bi_2Se_3 slabs, respectively, and the corresponding Bi_2Se_3 slabs in the middle are with six QLs. (b,d,f) Closest to Fermi RDOS for these sandwich slabs. The black dashed vertical lines are the boundaries between In_2Se_3 and Bi_2Se_3, and the regions between black and red dashed lines are the top and bottom QLs in the Bi_2Se_3 slab. The green and blue bars represent the In_2Se_3 and Bi_2Se_3 slab regions, respectively.

Se states (Figure 4b,e), so the sign of total parity for all of the occupied bands changes, and the system transfers into a topological nontrivial phase. However, the variance of the near-Fermi band structure due to Sb_2Se_3−Bi_2Se_3 interaction can lead to distinct band inversion pictures, as shown in Figure 4c,g. In the d3S−B decoupled junction, the Se1 state from Bi_2Se_3 becomes the conduction band (Figure 4e). Bi_2Se_3 and Sb_2Se_3 retain their topologically trivial and nontrivial nature, respectively. In contrast, for the 3S−B coupled junction, the Se2 state from Sb_2Se_3 rises to the conduction band (Figure 4b). The parity for Sb_2Se_3 becomes negative, while that for Bi_2Se_3 becomes positive. Therefore, the roles of the two materials exchange and the topological phase transition happens.

For the In_2Se_3−Bi_2Se_3 heterojunction, the situation is completely different (Figure 4h−j). The Se orbital (labeled Se3) and the In orbital of In_2Se_3 locate far from the Se1 and Bi orbitals of Bi_2Se_3 (Figure 4h,i). The coupling between Se3 and Se1 or between In and Bi is very weak. Therefore, In_2Se_3 coating has little influence on the topological property, and the band inversion picture is similar to the vacuum−Bi_2Se_3 system (Figure 4j).

The detailed mechanism of the "bulk-like" state exceeds the capability of *ab initio* simulation. A possible reason is that the Bi and Se2 states involved in the band inversion locate in different materials. On one hand, Sb_2Se_3 is in a nontrivial phase, so the topological state exists and crosses the vacuum−Sb_2Se_3 interface.

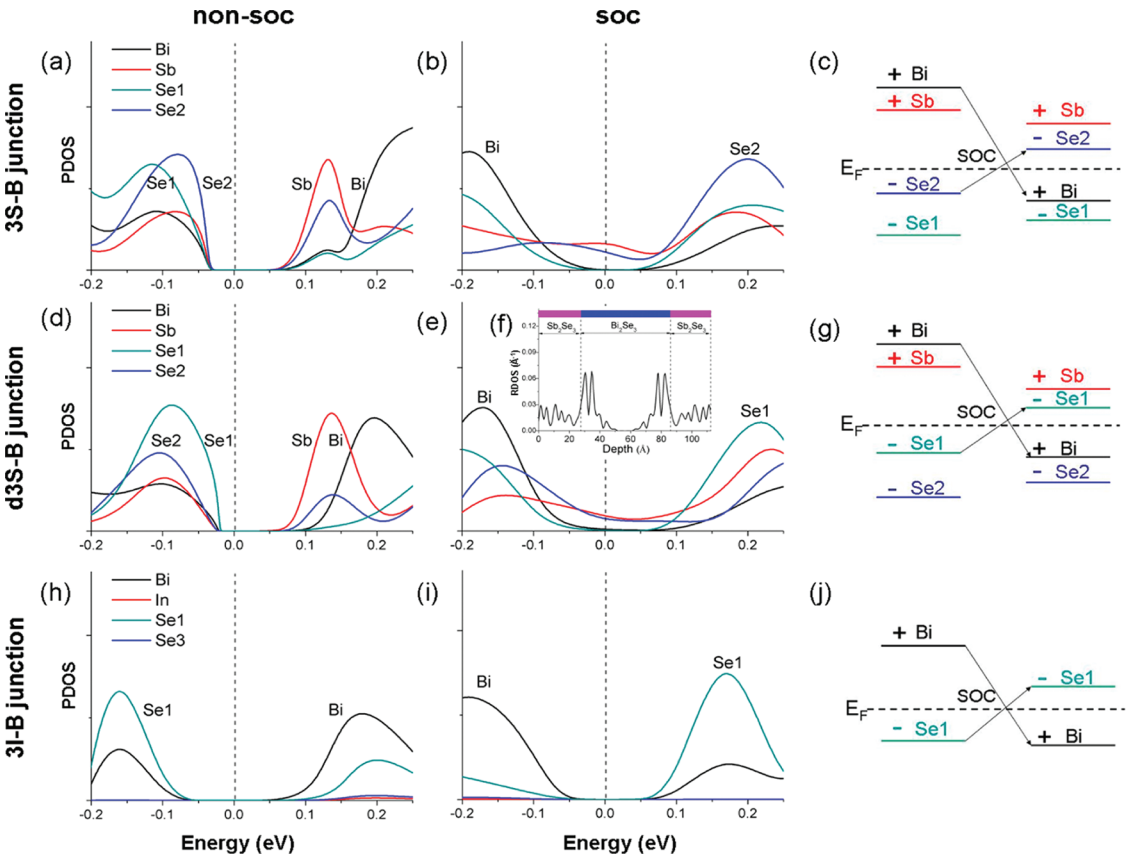

Figure 4. Atomic orbital projected density of state (PDOS) in energy space, without or with spin−orbit coupling (SOC) effect. Here, the partial density of state contributed by atom *m*'s orbital is obtained by integrating in k-space that very close to the Γ point $N_m(\varepsilon) = \int_{|\vec{k}|\leq(\pi/40a)} n_m(\varepsilon,\vec{k})d\vec{k}$, where *a* is the lattice constant, $n_m(\varepsilon,\vec{k}) = \Sigma_{i=s,p}|\langle\phi_{i,m}|\psi(\varepsilon,\vec{k})\rangle|^2$, and $\phi_{i,m}$ is the wave function of atom *m*'s orbital while $\psi(\varepsilon,\vec{k})$ is the total wave function. (a,d,h) When turning off the SOC effect, the PDOS for Bi (black), Sb (red), In (red), Se in Bi_2Se_3 (Se1, green), Se in Sb_2Se_3 (Se2, blue), and Se in In_2Se_3 (Se3, blue) near the Fermi level in three kinds of heterojunctions: 3S−B, d3S−B, and 3I−B junctions. Here, the atoms that we choose for PDOS calculation all locate on the center of Bi_2Se_3, Sb_2Se_3, or In_2Se_3 slabs. The dashed vertical line shows the position of the Fermi energy. (b,e,i) When turning on the SOC effect, the PDOS of state near the Fermi level in three kinds of heterojunctions. (c,g,j) Schematic pictures of the band inversion mechanism caused by the SOC effect in three kinds of heterojunctions. (f) Closest to Fermi RDOS for the d3S−B junction. The purple and blue bars represent the Sb_2Se_3 and Bi_2Se_3 slab regions.

On the other hand, due to strong coupling and the spatially mismatched band inversion, the topological state will be a mixture of all the bulk orbital states near the Fermi level, |Se2⟩ and |Sb⟩ on the conduction band and |Bi⟩ and |Se1⟩ on valence band, which indicates that this state has a real-space distribution in both materials. Therefore, this state should spread across the whole region of Sb_2Se_3 slabs. The detailed theoretical research, using an analytic method, is ongoing.

CONCLUSIONS

In conclusion, we have investigated Sb_2Se_3−Bi_2Se_3 heterostructures. Topological states migrate from nontrivial Bi_2Se_3 to trivial Sb_2Se_3, and surprising topological states with bulk-like spatial distribution were discovered, even when the thickness of Sb_2Se_3 extends to ∼6 nm. These states are distinct from topological surface states. Our results change the existing viewpoint that the topological surface state always appears locally at the interface within a couple of QLs between the trivial and nontrivial phase and shows an example of exotic phenomenon in TI-based heterostructures. On the other hand, the deformability and expansibility of the topological state will also give inspiration to experiment, such as in electronic devices, because the surface or boundary restriction can be eliminated, and the exciting features related to this state can be utilized in a wider range.

COMPUTATIONAL METHODS

All of the simulation systems are slab geometry. Fully self-consistent first-principle calculations, including atomic spin−orbit coupling, were performed using the Vienna Ab Initio Simulation Package (VASP) in the framework of density functional theory (DFT).[35,36] The projector-augmented wave (PAW) pseudopotential[37] was adapted, and the GGA exchange-correlation function was described by Perdew−Burke−Ernzerhof (PBE).[38] To guarantee convergence, we used 350 eV for the

cutoff energy of the plane-wave basis. The vacuum area with a thickness of more than 20 Å was used to separate the periodic images in the *z*-direction, which is wide enough to avoid any artificial interaction between images after our tests. All of the nanoslabs are infinite and periodic in the other two dimensions. The lattice constants for Bi_2Se_3 and In_2Se_3 are taken from experimental data,[32,39] and the lattice constants for Sb_2Se_3 come from previous theoretical study due to the lack of experimental demonstration.[5] In the $x-y$ plane, the lattice constants are a_0 = 4.138, 4.076, and 4.000 Å for Bi_2Se_3, Sb_2Se_3, and In_2Se_3, respectively. Therefore, Bi_2Se_3, Sb_2Se_3, and In_2Se_3 have quite similar lattice constant, and the lattice mismatch in the $x-y$ plane is only ~1.5% in the $Sb_2Se_3-Bi_2Se_3$ heterojunction and ~3.5% in the $In_2Se_3-Bi_2Se_3$ heterojunction. Both the small lattice mismatch and the weak van der Waals interaction between QLs suggest that the $Bi_2Se_3-Sb_2Se_3$ and $In_2Se_3-Bi_2Se_3$ heterostructures should have little lattice stress and can serve as good model systems for our investigation. For the heterojunction simulations, the in-plane lattice constants are chosen as that of Bi_2Se_3, a = 4.138 Å.

For slab systems, the Brillouin zone (BZ) is two-dimensional, and there are three non-equivalent time-reversal invariant momentum (TRIM) points (0, 0), (π, π), and (π, 0), named Γ, T1, and T2, respectively. Here, all of the band structures are plotted along the $T1-\Gamma-T2$ line.

Conflict of Interest: The authors declare no competing financial interest.

Acknowledgment. Y.C. acknowledges the support from the Keck Foundation, DARPA MESO project (No. N66001-11-1-4105) and King Abdullah University of Science and Technology (KAUST) Investigator Award (No. KUS-I1-001-12). The authors acknowledge the National Energy Research Scientific Computing Center (NERSC) and KAUST for computer time. Z.Z. acknowledges partial support from National Nanotechnology Infrastructure Network (NNIN).

REFERENCES AND NOTES

1. Bernevig, B. A.; Hughes, T. L.; Zhang, S. C. Quantum Spin Hall Effect and Topological Phase Transition in HgTe Quantum Wells. *Science* **2006**, *314*, 1757–1761.
2. König, M.; Wiedmann, S.; Brüne, C.; Roth, A.; Buhmann, H.; Molenkamp, L. M.; Qi, X. L.; Zhang, S. C. Quantum Spin Hall Insulator State in HgTe Quantum Wells. *Science* **2007**, *318*, 766–770.
3. Fu, L.; Kane, C. L.; Mele, E. J. Topological Insulators in Three Dimensions. *Phys. Rev. Lett.* **2007**, *98*, 106803.
4. Fu, L.; Kane, C. L. Topological Insulators with Inversion Symmetry. *Phys. Rev. B* **2007**, *76*, 045302.
5. Zhang, H. J.; Liu, C. X.; Qi, X. L.; Dai, X.; Fang, Z.; Zhang, S. C. Topological Insulators in Bi_2Se_3, Bi_2Te_3 and Sb_2Te_3 with a Single Dirac Cone on the Surface. *Nat. Phys.* **2009**, *5*, 438–442.
6. Hsieh, D.; Qian, D.; Wray, L.; Xia, Y.; Hor, Y. S.; Cava, R. J.; Hasan, M. Z. A Topological Dirac Insulator in a Quantum Spin Hall Phase. *Nature* **2008**, *452*, 970–974.
7. Hasan, M. Z.; Kane, C. L. C. L. Colloquium: Topological Insulators. *Rev. Mod. Phys.* **2010**, *82*, 3045–3067.
8. Day, C. Exotic Spin Textures Show up in Diverse Materials. *Phys. Today* **2009**, *62*, 12–13.
9. Hsieh, D.; Xia, Y.; Qian, D.; Wray, L.; Dil, J. H.; Meier, F.; Osterwalder, J.; Patthey, L.; Checkelsky, J. G.; Ong, N. P.; *et al.* A Tunable Topological Insulator in the Spin Helical Dirac Transport Regime. *Nature* **2009**, *460*, 1101–1105.
10. Hsieh, D.; Xia, Y.; Wray, L.; Qian, D.; Pal, A.; Dil, J. H.; Osterwalder, J.; Meier, F.; Bihlmayer, G.; Kane, C. L.; *et al.* Observation of Unconventional Quantum Spin Textures in Topological Insulators. *Science* **2009**, *323*, 919–922.
11. Chen, Y. L.; Analytis, J. G.; Chu, J. H.; Liu, Z. K.; Mo, S. K.; Qi, X. L.; Zhang, H. J.; Lu, D. H.; Dai, X.; Fang, Z.; *et al.* Experimental Realization of a Three-Dimensional Topological Insulator, Bi_2Te_3. *Science* **2009**, *325*, 178–181.
12. Xia, Y.; Wray, L.; Qian, D.; Hsieh, D.; Pal, A.; Lin, H.; Bansil, A.; Grauer, D.; Hor, Y.; Cava, R.; Hasan, M. Z. Observation of a Large-Gap Topological-Insulator Class with a Single Dirac Cone on the Surface. *Nat. Phys.* **2009**, *5*, 398–402.
13. Kroemer, H. Theory of a Wide-Gap Emitter for Transistors. *Proc. IEEE* **1957**, *45*, 1535–1537.
14. Kroemer, H. A Proposed Class of Heterojunction Injection Lasers. *Proc. IEEE* **1959**, *51*, 1782–1784.
15. Alferov, Z. I.; Andreev, V. M.; Korol'kov, V. I.; Trat'yakov, D. N.; Tuchkevich, V. M. High-voltage $p-n$ Junctions in $Ga_xAl_{1-x}As$ Crystals. *Sov. Phys. Semicond.* **1968**, *1*, 1313–1314.
16. Alferov, Z. I.; Andreev, V. M.; Korol'kov, V. I.; Portnoi, E. L.; Tret'yakov, D. N. Injection Properties of *n*-$Al_xGa_{1-x}As$-*p*-GaAs Heterojunctions. *Sov. Phys. Semicond.* **1969**, *2*, 843–844.
17. Alferov, Z. I.; Andreev, V. M.; Korol'kov, V. I.; Portnoi, E. L.; Tret'yakov, D. N. Coherent Radiation of Epitaxial Heterojunction Structures in the AlAs-GaAs System. *Sov. Phys. Semicond.* **1969**, *2*, 1289–1291.
18. Faist, J.; Capasso, F.; Sivco, D. L.; Sirtori, C.; Hutchinson, A. L.; Cho, A. Y. Quantum Cascade Laser. *Science* **1994**, *264*, 553–556.
19. Tsang, W. T. Extremely Low Threshold (AlGa)As Graded-Index Waveguide Separate-Confinement Heterostructure Lasers Grown by Molecular Beam Epitaxy. *Appl. Phys. Lett.* **1982**, *40*, 217–219.
20. Hafez, W.; Feng, M. Experimental Demonstration of Pseudomorphic Heterojunction Bipolar Transistors with Cutoff Frequencies above 600 GHz. *Appl. Phys. Lett.* **2005**, *86*, 152101.
21. Istrate, E.; Sargent, E. H. Photonic Crystal Heterostructures and Interfaces. *Rev. Mod. Phys.* **2006**, *78*, 455–481.
22. Sakaki, H. Velocity-Modulation Transistor (VMT)—A New Field-Effect Transistor Concept. *Jpn. J. Appl. Phys., Part 2* **1982**, *21*, L381–L383.
23. Capasso, F.; Sen, S.; Beltram, F.; Lunardi, L. M.; Vengurlekar, A. S.; Smith, P. R.; Shah, N. J.; Malik, R. J.; Cho, A. Y. Quantum Functional Devices: Resonant-Tunneling Transistors, Circuits with Reduced Complexity, and Multiple-Valued Logic. *IEEE Trans. Electron Devices* **1989**, *36*, 2065–2081.
24. Teo, J. C. Y.; Kane, C. L. Topological Defects and Gapless Modes in Insulators and Superconductors. *Phys. Rev. B* **2010**, *82*, 115120.
25. Ran, Y.; Zhang, Y.; Vishwanath, A. One-Dimensional Topologically Protected Modes in Topological Insulators with Lattice Dislocations. *Nat. Phys.* **2009**, *5*, 298–303.
26. Qi, X. L.; Li, R. D.; Zang, J. D.; Zhang, S. C. Inducing a Magnetic Monopole with Topological Surface States. *Science* **2009**, *323*, 1184–1187.
27. Fu, L.; Kane, C. L. Superconducting Proximity Effect and Majorana Fermions at the Surface of a Topological Insulator. *Phys. Rev. Lett.* **2008**, *100*, 096407.
28. Cook, A.; Franz, M. Majorana Fermions in Proximity-Coupled Topological Insulator Nanoribbons. *Phys. Rev. B* **2011**, *84*, 201105.
29. Qi, X. L.; Hughes, T. L.; Zhang, S. C. Topological Field Theory of Time-Reversal Invariant Insulators. *Phys. Rev. B* **2008**, *78*, 195424.
30. Zhang, W.; Yu, R.; Zhang, H. J.; Dai, X; Fang, Z. First Principles Studies on 3-Dimentional Strong Topological Insulators: Bi_2Te_3, Bi_2Se_3 and Sb_2Te_3. *New J. Phys.* **2010**, *12*, 065013.
31. Eremeev, S. V.; Landolt, G.; Menshchikova, T. V.; Slomski, B; Koroteev, Y. M.; Aliev, Z. S.; Babanly, M. B.; Henk, J; Ernst, A.; Patthey, L.; *et al.* Atom-Specific Spin Mapping and Buried Topological States in a Homologous Series of Topological Insulators. *Nat. Commun.* **2012**, *3*, 635–641.
32. Wyckoff, R. W. G. *Crystal Structures*; John Wiley and Sons: New York, 1964; Vol. 2.
33. Liu, C. X.; Zhang, H. J.; Yan, B. H.; Qi, X. L.; Frauenheim, T.; Dai, X.; Fang, Z.; Zhang, S. C. Oscillatory Crossover from Two Dimensional to Three Dimensional Topological Insulators. *Phys. Rev. B* **2010**, *81*, 041307.
34. Zhang, Y.; He, K.; Chang, C. Z.; Song, C. L.; Wang, L. L.; Chen, X.; Jia, J. F.; Fang, Z.; Dai, X.; Shan, W. X.; *et al.* Crossover of the Three-Dimensional Topological Insulator Bi_2Se_3 to the Two-Dimensional Limit. *Nat. Phys.* **2010**, *6*, 584–588.

35. Kresse, G.; Hafner, J. *Ab Initio* Molecular Dynamics for Open-Shell Transition Metals. *Phys. Rev. B* **1993**, *48*, 13115.
36. Kresse, G.; Furthmuller, J. Efficient Iterative Schemes for *Ab Initio* Total-Energy Calculations Using a Plane-Wave Basis Set. *Phys. Rev. B* **1996**, *54*, 11169.
37. Blochl, P. Projector Augmented-Wave Method. *Phys. Rev. B* **1994**, *50*, 17953.
38. Perdew, J. P.; Burke, K.; Ernzerhof, M. Generalized Gradient Approximation Made Simple. *Phys. Rev. Lett.* **1996**, *77*, 3865.
39. Ye, J.; Soeda, S.; Nakamura, Y.; Nittono, O. Crystal Structures and Phase Transformation in In_2Se_3 Compound Semiconductor. *Jpn. J. Appl. Phys.* **1998**, *37*, 4264–4271.